Journal of Thermal Biology 113 (2023) 103477

Contents lists available at ScienceDirect

Journal of Thermal Biology

journal homepage: www.elsevier.com/locate/jtherbio

Finite element model of female thermoregulation with geometry based on medical images

Michael P. Castellani [a,b,*], Timothy P. Rioux [b], John W. Castellani [b], Adam W. Potter [b], Sean R. Notley [c], Xiaojiang Xu [b,**]

[a] Oak Ridge Institute for Science and Education (ORISE), USA
[b] Thermal and Mountain Medicine Division, U.S. Army Research Institute of Environmental Medicine, USA
[c] Defence Science and Technology Group, Australia

ARTICLE INFO

Keywords:
Bio-heat transfer
Simulation
Heat strain
Finite element method
Control of body temperature
Thermal physiology

ABSTRACT

Introduction: this study describes the development of a female finite element thermoregulatory model (FETM)
Method: the female body model was developed from medical image datasets of a median U.S. female and was constructed to be anatomically correct. The body model preserves the geometric shapes of 13 organs and tissues, including skin, muscles, fat, bones, heart, lungs, brain, bladder, intestines, stomach, kidneys, liver, and eyes. Heat balance within the body is described by the bio-heat transfer equation. Heat exchange at the skin surface includes conduction, convection, radiation, and sweat evaporation. Vasodilation, vasoconstriction, sweating, and shivering are controlled by afferent and efferent signals to and from the skin and hypothalamus.
Results: the model was validated with measured physiological data during exercise and rest in thermoneutral, hot, and cold conditions. Validations show the model predicted the core temperature (rectal and tympanic temperatures) and mean skin temperatures with acceptable accuracy (within 0.5 °C and 1.6 °C, respectively)
Conclusion: this female FETM predicted high spatial resolution temperature distribution across the female body, which provides quantitative insights into human thermoregulatory responses in females to non-uniform and transient environmental exposure.

1. Introduction

Models of human thermoregulation describe heat balance within a body and heat exchange with the environment, using first principles of heat transfer and physiology. The autonomic mechanisms of thermoregulation in humans act as a negative feedback control system, which regulates body temperature through vasodilation, vasoconstriction, sweating, and shivering heat production (Charkoudian et al., 2017). Models have been developed and used widely for various applications; for example, evaluation of hypothermia or hyperthermia treatment procedures in clinical settings (Skok et al., 2020; Silva et al., 2018; Pereira et al., 2016), assessment of thermal comfort in building and automotive environments (Zhang et al., 2001; Koelblen et al., 2018; Enescu 2019; Fiala et al., 2010), research and development of personal protective ensembles (Xu et al. 2004, 2016; Choudhary et al., 2020), planning of search and rescue operations (Xu et al. 2008, 2011), and user-friendly software Apps for management of environmental stress (Xu et al., 2021; Potter et al., 2020; Kingma et al., 2021).

For convenience of model development, the human thermoregulatory system is conceptually divided into two subsystems: a passive and active system (Xu and Tikuisis 2014; Havenith and Fiala 2015; Stolwijk and Hardy 2011). The passive system represents the body anatomy and geometry as well as heat transfer processes, while the active system mathematically describes the dynamic thermoregulatory processes and mechanisms. A pioneering model of human thermoregulation was developed by Stolwijk and Hardy in the 1970s (Stolwijk and Hardy 2011). In this model, the human body was divided into six compartments, composed of one sphere and five cylinders. Each compartment was further divided into four layers to represent body anatomy: core, muscle, fat, and skin. Since then, numerous models of human thermoregulation have been developed using similar approaches with humans represented by one to sixteen cylindrical compartments (Tan et al., 2021; Stolwijk and Hardy 2011; Xu and Werner 1997; Wan and Fan

* Corresponding author. Thermal and Mountain Medicine Division, U.S. Army Research Institute of Environmental Medicine 10 General Greene Avenue, Natick, MA, 01760-5007, USA.
** Corresponding author.
E-mail addresses: michael.p.castellani2.ctr@health.mil (M.P. Castellani), xiaojiang.xu.civ@health.mil (X. Xu).

https://doi.org/10.1016/j.jtherbio.2023.103477
Received 28 October 2022; Received in revised form 4 January 2023; Accepted 5 January 2023
Available online 8 January 2023

Abbreviations

BDF	Backward differentiation formula
BSA	body surface area (m^2)
c_m	proportionality coefficient ($m^3 \cdot s^{-1} \cdot m^{-3} \cdot W^{-1}$)
C_p	specific heat at constant pressure ($J \cdot kg^{-1} \cdot K^{-1}$)
$C_{p,b}$	blood specific heat at constant pressure ($J \cdot kg^{-1} \cdot K^{-1}$)
CS	vasoconstriction signal (−)
DI	vasodilation signal ($m^3 \cdot s^{-1}\ m^{-3}$)
e_{hy}	hypothalamic error signal (°C)
e_s	skin error signal (°C)
E	sweat evaporation ($W \cdot m^{-2}$)
E_{dif}	heat flux from diffusion ($W \cdot m^{-2}$)
E_{max}	maximum sweat heat flux ($W \cdot m^{-2}$)
E_{rsw}	heat flux from sweat production ($W \cdot m^{-2}$)
f	view factor (−)
f_{cl}	clothing area factor (−)
FETM	finite element thermoregulatory model
h_c	convection coefficient ($W \cdot m^{-2} \cdot K^{-1}$)
h_{c0}	constant ($W \cdot m^{-2} \cdot K^{-1}$)
h_e	evaporative coefficient ($W \cdot m^{-2} \cdot Pa^{-1}$)
h_r	radiative coefficient ($W \cdot m^{-2} \cdot K^{-1}$)
LR	Lewis relation ($°C \cdot Pa^{-1}$)
m	constant in calculating h_c (−)
n	direction normal to surface (m)
P_a	ambient vapor pressure (Pa)
$P_{sk,s}$	skin vapor pressure (Pa)
Q_{ex}	regional exercise metabolic rate ($W \cdot m^{-3}$)
$Q_{EX_{tot}}$	total exercise metabolic heat (W)
Q_{SH}	regional shivering metabolic rate ($W \cdot m^{-3}$)
$Q_{SH_{tot}}$	total shivering metabolic heat (W)
Q_{tot}	total metabolic heat production (W)
Q_0	basal metabolic rate ($W \cdot m^{-3}$)
RH	relative humidity (%)
R_{cl}	intrinsic clothing thermal resistance ($m^2 \cdot °C \cdot W^{-1}$)
R_{ecl}	intrinsic clothing vapor resistance ($m^2 \cdot Pa \cdot W^{-1}$)
R_{resp}	respiratory heat loss (W)
t	time (s, min)
T	temperature (°C)
T_a	ambient temperature (°C)
T_b	blood temperature (°C)
T_{hy}	hypothalamus temperature (°C)
$T_{hy,set}$	thermoneutral hypothalamus temperature, set point (°C)
T_r	radiative temperature (°C)
T_s	skin temperature (°C)
T_{ms}	mean skin temperature (°C)
$T_{ms,set}$	thermoneutral mean skin temperature, set point (°C)
T_0	operative temperature (°C)
v	air velocity ($m \cdot s^{-1}$)
V	volume (m^3)
V_b	blood volume (m^3)
XCAT	Extended Cardiac-Torso
$\%BF$	percent body fat (%)
α_{DI}	vasodilation distribution factor (−)
α_{EX}	exercise distribution factor (−)
α_{SH}	shiver distribution factor (−)
α_{SW}	sweat distribution factor (−)
β	countercurrent heat exchange factor (−)
ε	emissivity (−)
λ	thermal conductivity ($W \cdot m^{-1} \cdot K^{-1}$)
ω	blood flow rate ($m^3 \cdot s^{-1} \cdot m^{-3}$)
ω_0	basal blood flow rate ($m^3 \cdot s^{-1} \cdot m^{-3}$)
ω_m	muscle blood flow rate ($m^3 \cdot s^{-1} \cdot m^{-3}$)
ω_{m0}	basal muscle blood flow rate ($m^3 \cdot s^{-1} \cdot m^{-3}$)
ω_s	skin blood flow rate ($m^3 \cdot s^{-1} \cdot m^{-3}$)
ω_{s_0}	basal skin blood flow rate ($m^3 \cdot s^{-1} \cdot m^{-3}$)
ρ	density ($kg \cdot m^{-3}$)
ρ_b	blood density ($kg \cdot m^{-3}$)
σ	Stefan-Boltzmann constant ($W \cdot m^{-2} \cdot K^{-4}$)

2008; Xu et al., 2005; Tanabe et al., 2002; Huizenga et al., 2001; Karaki et al., 2013; Fiala et al., 2001; Takahashi et al., 2021). Some models have sought to better approximate the human body by using various compartment shapes (e.g., spheres, ellipsoids, or truncated circular cones) (Lai and Chen 2016; Ferreira and Yanagihara 2009; Kang et al., 2019; Sun et al., 2012). Recently, anatomically, and geometrically correct models of human thermoregulation have been developed (Castellani et al., 2021; Unnikrishnan et al., 2021; Nelson et al., 2009), where human body meshes were derived from medical images. Advancements in passive systems of human thermoregulation models reflect the needs and necessities to develop better models and predict body temperatures at higher resolutions.

Sex differences in thermoregulation have been of on-going interest for decades (Gagnon and Kenny 2012; Yanovich et al., 2020; Stephenson and Kolka 1993). These studies attempted to determine if women and men regulate their temperature differently, if the differences are due to physiological differences or simply due to differences in physical characteristics, and if sex differences in thermoregulation result in differences in physical performance and affect female's capability to complete physically strenuous tasks. However, only very limited research efforts attempted to model sex differences in thermoregulation.

Most of the existing models are sex-neutral, that is, they do not distinguish between male or female. One model of human thermoregulation was developed for women with the passive system represented as one sphere and nine cylinders (Iyoho et al., 2017), which does not adequately represent differences in body morphology and composition between men and women. The active system equations for sweating and shivering were adjusted to take into account sex differences. Some studies have examined sex differences in temperature regulation during heat stress and found differences in sweat rates and core temperatures (Gagnon and Kenny 2011). However, overall, data do not support increased (or altered) risk of heat illness in women compared to men, since most differences occurred at the extremes of thermoregulatory responses. For example, women have lower maximal sweating rates than men, but heat dissipation via sweating at most relevant activity and environmental levels were similar between men and women (Gagnon and Kenny 2011; Yanovich et al., 2020; Mehnert et al., 2002). Similarly, sex differences in shivering heat production were observed during cold water immersion, but adjusting for sex was not necessary if the percent body fat and ratio between body surface area to mass were taken into account (Tikuisis et al., 2000). From the perspective of heat transfer, differences in body geometry and anatomy result in different

temperature distributions across the body, thus these differences are potential reasons for sex differences in thermoregulation that must be considered to optimize model prediction.

Recently, male medical image datasets were successfully used to develop anatomically correct male models of human thermoregulation (Castellani et al., 2021; Unnikrishnan et al., 2021; Nelson et al., 2009). The purpose of this study was to develop and validate a female finite element model of human thermoregulation using female image datasets from the Extended Cardiac-Torso (XCAT) Phantoms of Duke University.

2. Methods

The scheme of the female finite element thermoregulatory model (FETM) is shown in Fig. 1. This FETM consists of a passive system and an active system. The passive system is an anatomically realistic body model. The active system is a mathematical representation of the female thermoregulatory mechanisms which include vasodilation, vasoconstriction, sweating and shivering heat production. Skin blood flow, sweating, and shivering are regulated by the controlling signal from hypothalamus and skin, i.e., e_{hy} and e_s. The muscle blood flow is regulated during exercise and shivering. Details of the passive and active systems are described below.

Several assumption were made to simplify model development: 1) the temperature of venous blood exiting the tissues reaches equilibrium with surrounding tissues and thus venous temperature is equal to the tissue temperature; 2) the variation of the arterial blood temperatures was considered through the countercurrent heat exchange factor β; 3) the body has a central blood pool and the temperature of this pool was independent of location; 4) 100% of respiratory heat exchange occurs in the lungs.

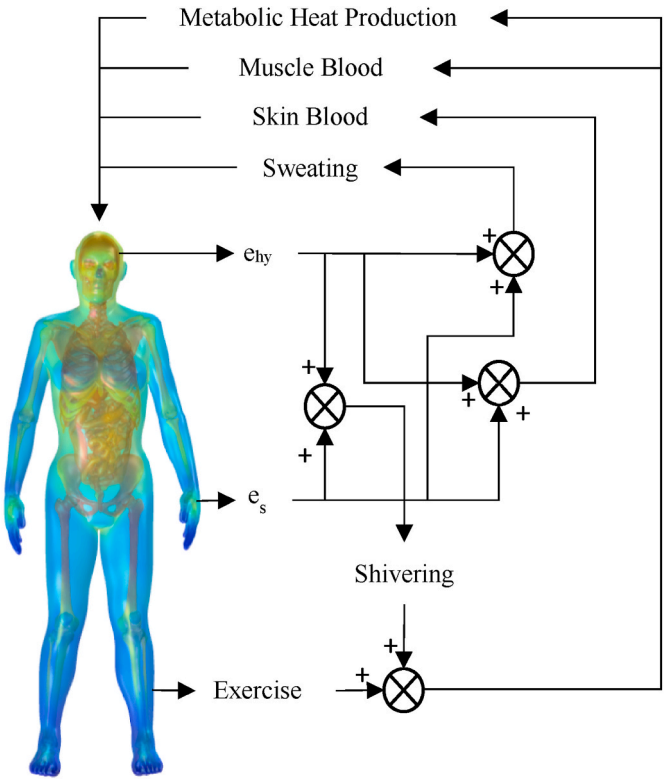

Fig. 1. Scheme of the female/women finite element thermoregulatory model.

2.1. Medical image dataset

Female medical image datasets have become available thanks to advances in medical imaging techniques, (e.g., Visible Human Project® (VHP) from National Library of Medicine (Ackerman 1999), Extended Cardiac-Torso (XCAT) Phantoms of Duke University (Segars et al., 2013), and Virtual Family (Christ et al., 2010)). Duke University's XCAT phantoms were developed for the purpose of medical research and simulations, and include highly detailed anatomies with images closely mirroring living people (Segars et al., 2013). The XCAT series includes a vast population of phantoms of varying anatomies for U.S. male and female adults.

2.2. Female anatomically realistic geometry

One of the XCAT phantoms was used to generate a female body mesh which represented the median U.S. adult female, 36 years old, 1.62m tall, and body mass of 66 kg. Image processing included several main steps: voxelization, segmentation, region separation and mesh generation. The workflow produced a pipeline where the image data was voxelized with an isotropic resolution of 1 mm (Castellani et al., 2021; Genc et al., 2013). Simpleware™ ScanIP (Synopsys, Mountain View, CA) was then used to segment the data into a CAD model. The data was segmented into objects representing various segmented regions and organs (see regions in Table 1 and organs in Table 2). The Simpleware™ FE module was then used to create the final volume mesh out of tetrahedral elements. The mesh underwent mesh independent tests and were optimized for simulation in COMSOL Multiphysics (COMSOL Inc., Burlington MA), a finite element analysis software. 4.0 mm was specified as the minimum edge length for the smallest/thinnest regions. The body consisted of 6.2 million tetrahedral elements. Fig. 2 shows the finite element body geometry, internal organs, and tissues. Table 1 shows the organ and tissue volume of various body regions.

Table 1
Volume of various body regions of the female model.

	Volume $m^3 \cdot 10^{-6}$						Surface Area m^2
	Viscera	Bone	Muscle	Fat	Skin	Total	
Head	1261	828	816	1098	285	4287	0.128
Torso	6836	2782	9893	15,198	1247	35,956	0.560
Upper arm	0	222	766	1726	300	3014	0.135
Lower arm	0	170	612	1035	229	2046	0.107
Hand	0	136	242	447	202	1031	0.096
Upper leg	0	836	5160	7721	810	14,526	0.369
Lower leg	0	499	1787	2406	434	5125	0.197
Foot	0	471	379	1260	285	2394	0.131
Total	8097	5947	19,654	30,890	3793	68,281	1.723

Table 2
Thermal properties and volumes for each organ.

Organs	λ W·m^{-1}·°C	ρ kg·m^{-3}	C_p J·kg^{-1}·°C^{-1}	Q_0 W·m^{-3}	ω_0 m^3·s^{-1}·m^{-3}	Volume m^3·10^{-6}
Skin	0.517	1085	3680	368.1	5.42E-04	3793
Fat	0.231	920	2300	368.3	7.32E-05	30,899
Muscle	0.617	1085	3800	684.1	4.39E-04	19,654
Bladder	0.480	930	3200	370.3	1.39E-04	186
Intestine	0.470	1085	3200	405.1	5.76E-03	1627
Stomach	0.510	960	3560	405.1	5.76E-03	331
Kidneys	0.480	1080	3600	23,889.0	5.19E-02	272
Lungs	0.280	560	3520	365.4	2.95E-02	2508
Liver	0.480	1080	3690	14,413.6	1.13E-02	1483
Heart	0.470	1080	3550	25,200.0	1.08E-01	615
Bones	0.750	1357	1700	368.3	0.00E-01	5950
Brain	0.527	1035	3550	15,000.0	8.79E-03	1246
Eyes	0.870	1022	3200	666.0	9.37E-07	15

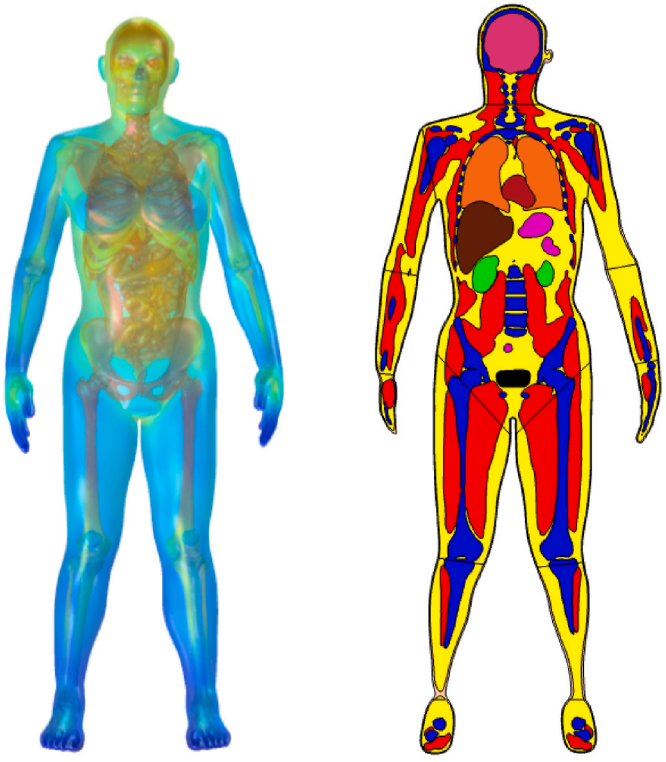

Fig. 2. Female body model after thermoneutral simulation (left), and cross section (right): skin (black outline), fat/connective tissue (yellow), muscle (red), brain (pink), bones (blue), lungs (orange), heart (dark red), liver (brown), stomach/intestines (magenta), kidneys (green), and bladder (black).

Table 3
Regional values for h_{c0} and h_r.

Region	h_{c0}	h_r
Head	10.1	4.5
Torso	10.1	4.5
Upper arm	10.1	4.5
Forearm	9.5	4.3
Hand	9.5	4.3
Thigh	11.1	4.5
Lower leg	11.1	4.7
Foot	11.1	4.7

Table 4
Regional distribution factors.

Region	α_{DI}	α_{SW}	α_{SH}	α_{EX}	β
Head	0.151	0.12	0.02	0.02	1.0
Torso	0.23	0.345	0.8	0.20	1.0
Upper arm	0.075	0.055	0.012	0.04	0.95
Forearm	0.08	0.066	0.08	0.04	0.9
Hand	0.134	0.055	0	0.01	0.8
Thigh	0.115	0.155	0.13	0.35	0.9
Lower leg	0.115	0.134	0.03	0.33	0.75
Foot	0.1	0.07	0	0.01	0.7

α_{DI}: distribution factor of the vasodilation; α_{SW}: distribution factor of sweat; α_{SH}: distribution factor of shivering heat production; β: counter-current coefficients.

2.3. Passive system

The passive system incorperates the geometric and anatomic characteristics and thermal properties. The bio heat equation was used to describe the heat transfer and heat balance within the body:

$$\rho C_p \frac{\partial T}{\partial t} = \lambda \nabla^2 T + Q_0 + Q_{SH} + Q_{EX} + \beta \omega \rho_b C_{p,b} (T_b - T)$$

where ρ is the density (kg·m^{-3}), C_p is the specific heat (J·kg^{-1}·°C^{-1}), T is temperature (°C), t is time (s), λ is the thermal conductivity (W·m^{-1}·°C^{-1}), ∇ is the gradient, Q_0 is the tissue basal metabolic rate (W·m^{-3}), Q_{SH} is the tissue shivering heat production rate (W·m^{-3}), Q_{EX} is the increased metabolic rate due to exercise (W·m^{-3}), β is the factor of countercurrent heat exchange between arterial blood and venous blood, ω is the blood flow rate (m^3·s^{-1}·m^{-3}), ρ_b is the blood density (kg·m^{-3}), $C_{p,b}$ is the specific heat of blood (J·kg^{-1}·°C^{-1}), and T_b is the blood temperature (°C). Table 2 shows the values for λ, ρ, C_p, Q_0, and ω_0. Thermal properties were adapted from the literature (Werner and Buse 1988; Nelson et al., 2009). The values for β are shown in Table 4. These values started as values similar to previous work and were refined to increase model accuracy. The left hand side of the bio heat equation describes how temperature changes over time. The right hand side of the equation describes how heat is transferred through conduction, metabolic heat production (e.g., shivering, exercise), and convection via blood flow.

The skin surface is the boundary of the model. Convection, radiation, and evaporation all contribute to the heat exchange at boundary and the boundary condition is described as:

$$-\lambda \frac{\partial T}{\partial n} = (h_c + h_r) \cdot (T_s - T_o) + E$$

where n is the normal to the boundary, h_c is the convection coefficient (W·m^{-2}·°C^{-1}), h_r is the radiation coefficient (W·m^{-2}·°C^{-1}), T_s is surface temperature (°C), T_o is operative temperature (°C), and E is heat loss by

sweat evaporation (W·m^{-2}). T_o is determined as (ASHRAE 2013):

$$T_o = \frac{T_a \bullet h_c + T_r \bullet h_r}{h_c + h_r}$$

where T_a is ambient temperature (°C), and T_r is radiative temperature of the environment (°C). For indoor condition without radiation sources, the T_r is considered the same as T_a. The equation (de Dear et al., 1997):

$$h_c = h_{c0} v^m$$

computes the convective coefficient. Here h_{c0} is a constant, v is the wind velocity (m·s^{-1}) and m is a constant. h_{c0} varies with body location and the values are shown in Table 3 (de Dear et al., 1997). The m is set to 0.56 when standing and 0.61 when sitting. The h_r is derived from Stefan-Boltzmann law and calculated by:

$$h_r = f \bullet \varepsilon \bullet \sigma \bullet \left[(T_s + 273.2)^2 + (T_r + 273.2)^2\right] \cdot (T_s + T_r + 546.3)$$

where f is view factor, ε is emissivity, and σ is the Stefan–Boltzmann constant ($5.67 \cdot 10^{-8}$ W m^{-2}·K^{-4}). However, h_r is traditionally treated as a constant for human-environment thermal responses (Xu and Tikuisis 2014; Xu et al., 2019). Thus, h_r is treated as a constant and only varies with respect to the body region. These values are shown in Table 3 (de Dear et al., 1997).

The equation for modelling blood temperature is described as:

$$V_b \frac{dT_b}{dt} = \int \beta \omega (T - T_b) dV$$

where V_b is the volume of the blood (m^3) and assumed to be 0.005 m^3 (5 L). This model assumes: 1) the body has a central blood pool, 2) this blood temperature is independent of the location, and 3) that blood temperature in the capillaries and veins is equal to the temperature of their neighboring tissues.

The model assumes that 100% of respiratory heat exchange occurs in the lungs. Convective and evaporative heat transfer occur when the respiratory track exchanges air with the environment. These values are in proportional to respiratory volume and increase when the body's metabolism increases. The respiratory heat loss is estimated by (Fanger 1982):

$$R_{resp} = 0.0014 Q_{tot} (34.0 - T_a) + 0.0173 Q_{tot} \left(5.87 - 10^{-3} P_a\right)$$

where R_{resp} is the respiratory heat loss (W), Q_{tot} is the total metabolic heat production (W), T_a is the ambient temperature (°C), and P_a is the ambient vapor pressure (Pa). The total metabolic rate Q_{tot} is calculated as:

$$Q_{tot} = \int Q_0 dV + Q_{SH_{tot}} + Q_{EX_{tot}}$$

where $Q_{SH_{tot}}$ is the total shivering heat production (W) and $Q_{EX_{tot}}$ is the increased metabolic heat production due to exercise (W).

2.4. Clothing

Clothing acts as insulation between the skin and environment, which reduces the heat exchange between the skin and environment when worn. Thus, the boundary equation in Eq. 2 must be altered. The boundary equation becomes:

$$-\lambda \frac{\partial T}{\partial n} = \frac{T_s - T_o}{R_{cl} + \frac{1}{f_{cl} \bullet (h_c + h_r)}} + E$$

where R_{cl} is the intrinsic clothing thermal resistance (m^2·°C·W^{-1}), and f_{cl} is the dimensionless clothing area factor expressed as the ratio of the clothing surface to body surface area. In addition, clothing affects evaporative heat loss also and this impact is described in Eq. 22.

The ambient environment controls the amount of heat that can be removed by the body through sweat. The maximum amount of evaporation calculated at any point in time is calculated by (ASHRAE 2013):

$$E_{max} = \frac{P_{sk,s} - P_a}{R_{ecl} + \frac{1}{f_{cl} \bullet h_e}}$$

where $E_{\max}$ is the maximum amount of heat lost through sweat (W·m^{-2}), $P_{sk,s}$ is the saturated vapor pressure at the skin, P_a is the vapor pressure of the ambient environment, R_{ecl} is the intrinsic clothing vapor resistance (m^2·Pa·W^{-1}), and f_{cl} is the dimensionless clothing area factor expressed as the ratio of the clothing surface to body, and h_e is the evaporative heat transfer coefficient (W·m^{-2} Pa^{-1}). The Lewis relation (LR) correlates h_e and h_c by:

$$h_e = LR \bullet h_c$$

where LR is the Lewis relation (°C·Pa^{-1}). Typically, LR is 16.5 °C·kPa^{-1} (ASHRAE 2013; Gagge and Gonzalez 2010).

2.5. Active system

The human thermoregulatory system regulates body temperature. It is simplified into three subsystems: sensor, integrator, and effector (Stolwijk and Hardy 2011). It is believed that the hypothalamic region of the brain has the most thermoreceptors. The skin has both cold and warm sensors which are dedicated to the detection of cold and warmth. These skin thermoreceptors send signals to the hypothalamus through the sympathetic nervous system. The integrator system takes in and combines the thermoreceptor signals and outputs effector commands. The effector system executes the commands (e.g., vasoconstriction, vasodilation, sweating, and shivering). The error signals from the sensors are described by:

$$e_{hy} = T_{hy} - T_{hy,set}$$

$$e_s = T_{ms} - T_{ms,set}$$

where e_{hy} is the error signal from the sensor in the hypothalamic region (°C), T_{hy} is the temperature in hypothalamic region (°C), $T_{hy,set}$ is the reference temperature for the hypothalamic region (°C), e_s is the error from all sensors of the skin (°C), T_{ms} is the mean skin temperature (°C), and $T_{ms,set}$ is the reference temperature for the mean skin temperature (°C). The reference temperatures are the hypothalamus or skin temperatures at thermoneutral conditions where error signals are zero. $T_{hy,set}$ and $T_{ms,set}$ are 37.1 °C and 33.4 °C respectively. These values are calculated from running a thermoneutral simulation defined as 29 °C, 40% relative humidity (RH), 0.18 m s^{-1} wind speed, and 92.3 W of metabolic heat production.

The amount of skin blood flow can change with vasodilation and vasoconstriction. They are calculated by the following equations, adapted from the Stolwijk model (Stolwijk and Hardy 2011):

$$DI = 113696 \cdot e_{hy} + 19480 \cdot e_s$$

$$CS = 1.1 \cdot \left(-e_{hy}\right) + 3.3 \cdot (-e_s)$$

$$\omega_s = \frac{\omega_{s_0} + \alpha_{DI} \cdot DI}{1 + CS}$$

where DI is the total efferent skin vasodilation signal (m^3·s^{-1}·m^{-3}), CS is a total efferent skin vasoconstriction signal (dimensionless), ω_s is the skin blood flow (m^3·s^{-1}·m^{-3}), ω_{s_0} is basal skin blood flow rate (m^3·s^{-1}·m^{-3}), and α_{DI} is a distribution factor of vasodilation. The values for α_{DI} are shown in Table 4. In these equations it is not possible to have "negative" vasoconstriction or vasodilation. This is avoided by setting negative values of DI and CS to zero.

When the body is cold, shivering heat production is activated. Heat production from shivering is determined by (Tikuisis and Giesbrecht

1999):

$$Q_{SH_{tot}} = \frac{147.7\cdot(-e_{hy}) + 44.6\cdot(-e_s) - 1.48\cdot(e_s)^2}{\sqrt{PBF}}\cdot BSA$$

where $Q_{SH_{tot}}$ is the metabolic heat from shivering (W), PBF is body fat percentage, and BSA is the body surface area (m^2). Negative values of are set to zero. $Q_{SH_{tot}}$ is then broken up regionally, this is calculated by:

$$Q_{SH} = \frac{\alpha_{SH}\cdot Q_{SH_{tot}}}{V_i}$$

where α_{SH} is a distribution factor of shivering heat production, and V_i is the muscle of segment (m^3). The values for α_{SH} can be found in Table 4.

$Q_{EX_{tot}}$ is usually measured or estimated from the mechanical output and mechanical efficiency. Then the increased heat production due to exercise in each region is calculated by:

$$Q_{EX} = \frac{\alpha_{EX}\cdot Q_{EX_{tot}}}{V_i}$$

where Q_{EX} is the regional exercise metabolic rate ($W\cdot m^{-3}$) and α_{EX} is a distribution factor of increased heat production due to exercise.

When muscle contractions increase and metabolic workload is higher, a greater amount of oxygen is needed; therefore, blood flow is increased. This increase is modeled as:

$$\omega_m = \omega_{m0} + c_m\cdot(Q_{SH} + Q_{EX})$$

where ω_{m0} is the basal blood flow rate of muscle ($m^3\cdot s^{-1}\cdot m^{-3}$), and c_m is the proportionality coefficient ($m^3\cdot s^{-1}\cdot m^{-3}\cdot W^{-1}$). The c_m was assumed to be about 1.39 $m^3\ s^{-1}\cdot W^{-1}$.

The body loses heat to the environment through evaporative heat loss. Evaporation is calculated by (ASHRAE 2013):

$$E = E_{dif} + E_{rsw}$$

where E_{dif} is the basal evaporation ($W\cdot m^{-2}$), and E_{rsw} is the evaporation of sweat regulated by human thermoregulatory system ($W\cdot m^{-2}$). E_{dif} is the evaporative heat loss caused by water diffusing to the environment from the skin. This is caused by the pressure gradient between the environment and skin. This heat exchange varies based off of the environmental temperature and ranges from 5.6 to 10.4 W m^{-2} when T_a changes from 15 to 30 °C (Lamke and Wedin 1971; Lamke et al., 1977). These two studies produced data that could be accurately explained by a piecewise function based off the ambient temperature. E_{dif} is calculated by:

$$E_{dif} = \begin{cases} 5.6 & T_a \le 15 \\ 5.6 + 0.0213(T_a - 15.0)^2 & 15 < T_a < 30 \\ 10.4 & T_a \ge 30 \end{cases}$$

Adapted from the Stolwijk model, E_{rsw} is the evaporative heat loss caused by secreted sweat (Stolwijk and Hardy 2011; Castellani et al., 2021):

$$E_{rsw} = \alpha_{SW}\cdot\left(150\cdot e_{hy} + 32\cdot e_s\right) + 100.0\frac{dT_{ms}}{dt}\cdot\frac{\left(\frac{dT_{ms}}{dt}\right)^6}{0.05^6 + \left(\frac{dT_{ms}}{dt}\right)^6}$$

where α_{SW} is the regional distribution factor of sweat, the term $\frac{dT_{ms}}{dt}$ is the instantaneous rate of change for the mean skin temperature and is set to zero when $\frac{dT_{ms}}{dt}$ is > 0 °C·min^{-1}. The values for α_{SW} can be found in Table 4. Negative values of E_{rsw} are set to zero.

2.6. Numerical methods and sensitivity analysis

The model was developed using the Bioheat Transfer Interface of the COMSOL Multiphysics Heat Transfer Module. All equations described above were implemented into the model as variables. The simulations use a linear discretization. An iterative solver is used to run stationary simulations. The backward differentiation formula (BDF) solver, an implicit solver, is used for dynamic simulations. A maximum time step of 1 min was chosen to reduce numerical error, however, COMSOL's adaptive methods could use time steps less than a minute.

The model predictions are affected by the thermal properties in Table 2. Sensitivity analysis was performed using hot and cold simulations to check how an error in the properties affect the model. The ambient conditions were: nude rest at 40 °C for 1 h and at 0 °C for 1 h. Each simulation was repeated where one group of the thermal properties was changed by ±10%, while holding the other properties constant. After 1 h, the greatest rectal temperature difference was 0.08 °C, greatest heart temperature difference was 0.14 °C, and the greatest skin temperature difference was 0.23 °C. This sensitivity analysis demonstrated that the model is only slightly affected by errors in the thermal properties.

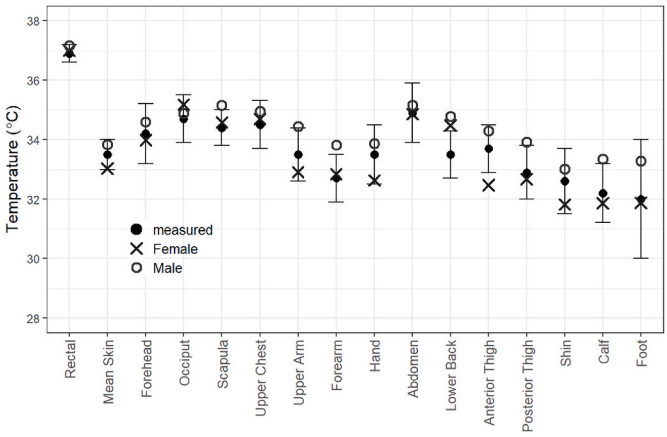

Fig. 3. Measured, predicted female and predicted male rectal, mean skin, and local temperatures in a thermoneutral environment of 25.6 °C, RH 50% and wind speed of 0.1 m s^{-1} *(Olesen and Fanger 1973)*.

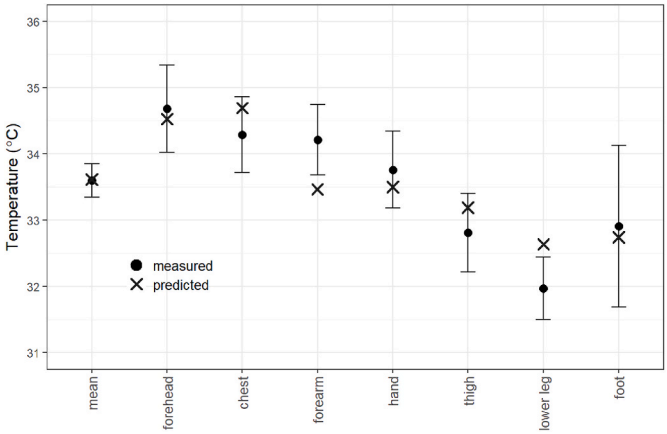

Fig. 4. Predicted and measured skin temperatures in 18 females in a thermoneutral environment of 26.7 °C (Nonaka et al., 2009).

3. Results

Model validation was done by comparing the predicted values with observed values for body core and mean and local skin temperatures from six datasets. In analyzing the model performance we considered a difference of 0.5 °C in core temperature and a 1.6 °C difference in mean skin temperature to be acceptable (Haslam and Parsons 1994).

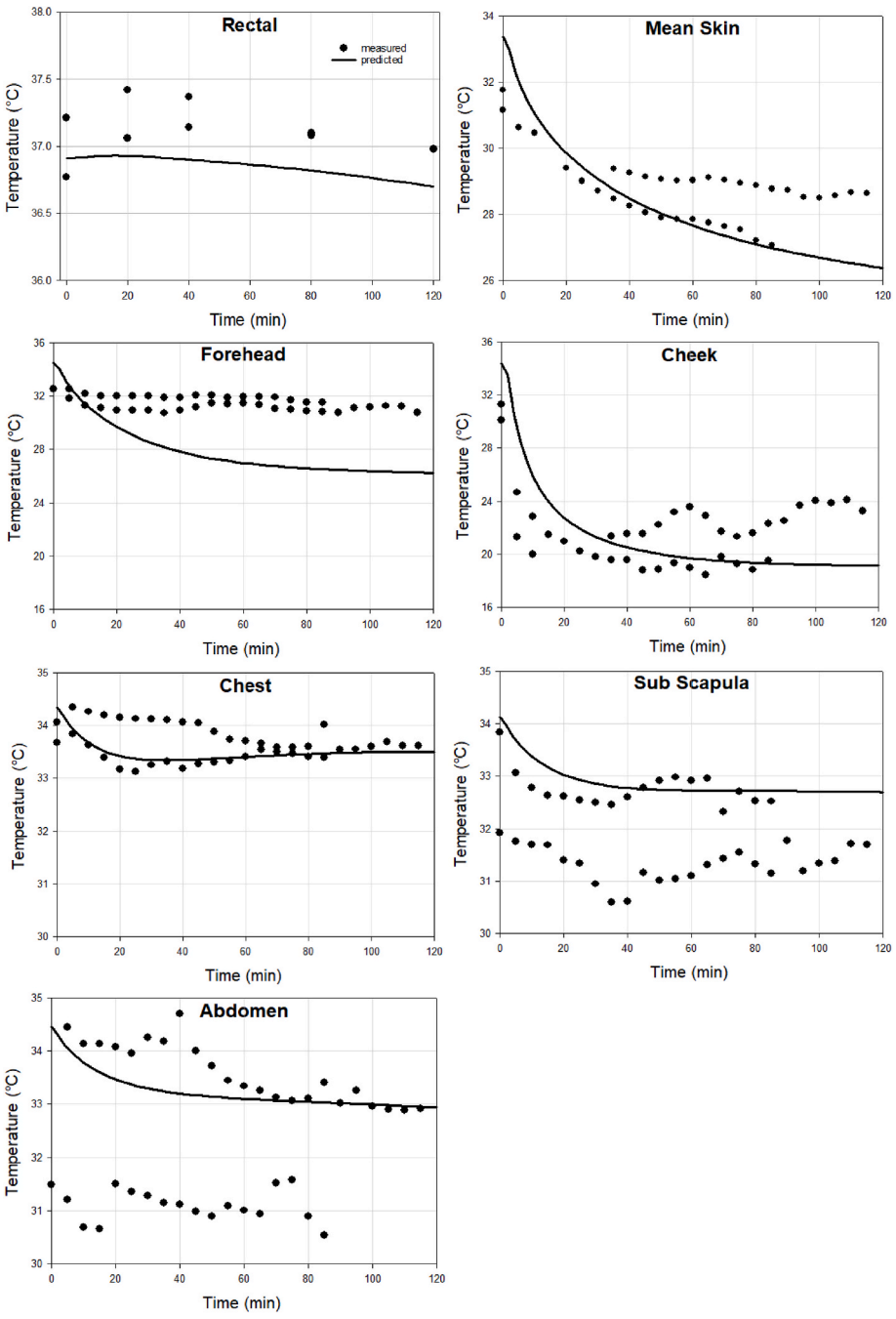

Fig. 5. Predicted and measured rectal, mean, and local skin temperatures while wearing cold weather clothing ensemble and sitting in 0.48 °C, RH 51%, 1.34 m s^{-1} (*Castellani* et al. *2018*).

3.1. Thermoneutral environments with office clothing

Thirty-two female and male volunteers rested in an environment of 25.6 °C, 50% RH, and a wind speed of 0.1 m s^{-1} for 2.5 h to obtain thermoneutral skin temperatures (Olesen and Fanger 1973). Volunteers wore office clothing with an estimated intrinsic thermal resistance of 0.6 clo and estimated intrinsic evaporative resistance of 20.7 m^2 Pa·W^{-1}. The temperature was measured at 14 different locations on the skin as well as the rectal temperature. The predicted temperatures as well as the measured mean ± standard deviation (SD) values are shown in Fig. 3. All predicted values are within 1 SD of the measured temperature except the anterior thigh. The predicted male values are also shown in Fig. 3 for comparison (Castellani et al., 2021). The error in the rectal temperature was 0.09 °C and the root mean squared deviations (RMSD) of the skin temperatures was 0.57 °C.

Eighteen female volunteers between 21 and 24 years old rested in a thermoneutral environment of 26.7 °C, RH50% and 0.1 m/s for 60 min (Nonaka et al., 2009). Local skin temperatures were taken at 7 locations. The predicted temperatures as well as the measured mean ± SD are shown in Fig. 4. All predicted values were within 1 SD of the measured temperature except for the forearm and lower leg. The forearm was 0.21 °C less than 1 SD and the lower leg was 0.19 °C greater than 1 SD of the measured temperature. The RMSD of the measured skin temperatures was 0.42 °C.

3.2. Transient cold conditions

Two female volunteers sat in an environment of 0.48 ± 0.53 °C, 51%

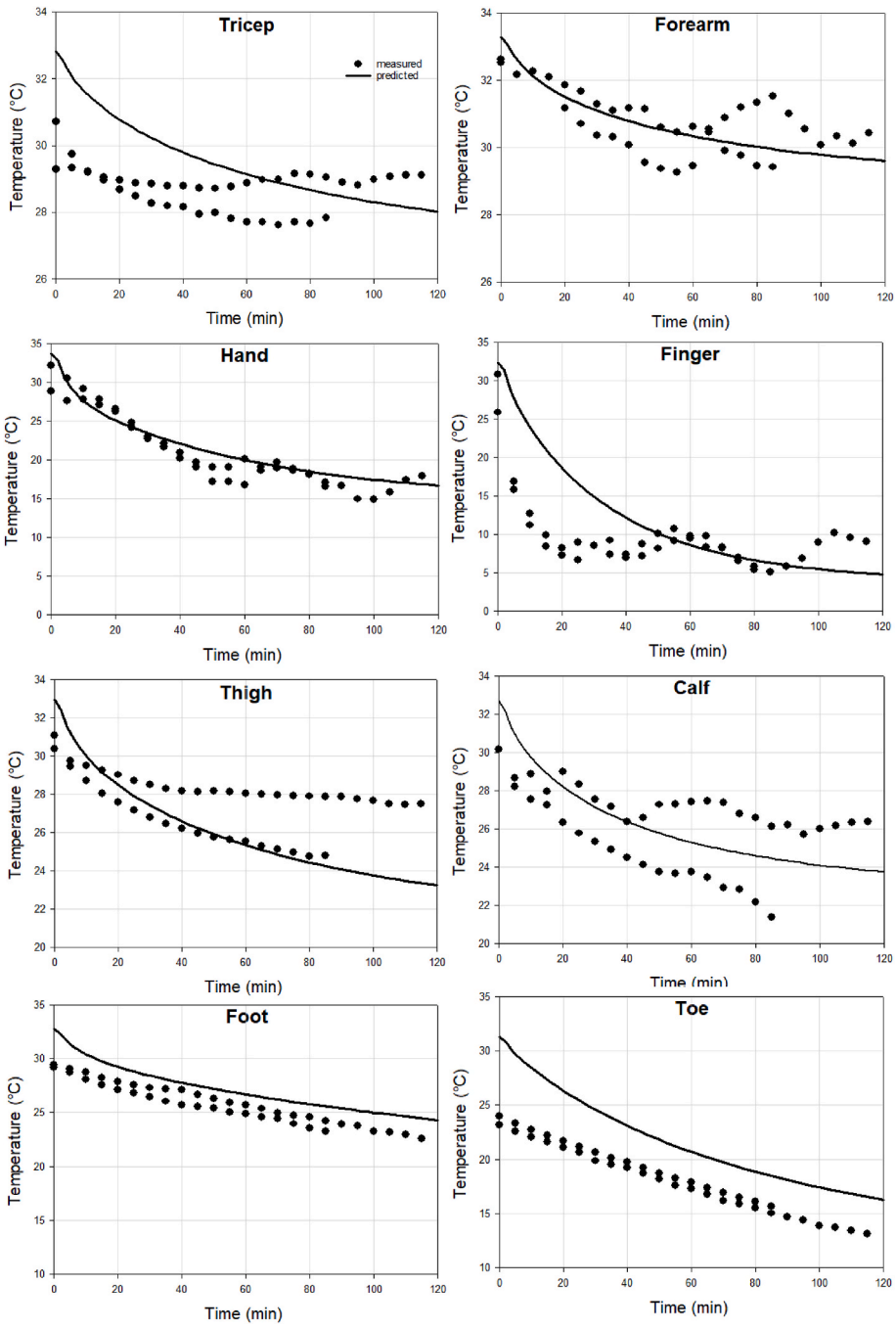

Fig. 6. Predicted and measured local arm, hand, and leg temperatures while wearing cold weather clothing ensemble and sitting in 0.48 °C, RH 51%, 1.34 m s^{-1} (*Castellani* et al. *2018*).

RH, and 1.34 m s^{-1} wind speed for 2 h (Castellani et al., 2018). One of the two volunteers only completed 85 min of exposure. Volunteers wore 3 layers of the U.S. Army extended cold weather clothing system, a fleece watch cap, wool socks, and winter boots. Skin temperatures were measured at 13 sites: forehead, cheek, chest, sub scapula, abdomen, tricep, forearm, hand, finger, thigh, calf, foot, and toe. Additionally, rectal temperature was measured using a thermometer pill logged at times 0, 20, 40, 80, and 120 min. Predicted and measured values are shown in Fig. 5 and Fig. 6. Predicted rectal temperature was slightly lower than the measured values, but the differences were less than 0.28 °C. Most of the predicted skin temperatures agreed with the range of measured values. The patterns seen in the fingers and cheek are likely indicative of cold-induced vasodilation, which is not yet incorporated into the model. Overall, the predicted rectal and mean skin temperatures had a RMSD of 0.28 and 1.24 °C respectively.

3.3. Transient hot conditions

Seven female volunteers were exposed to an environment of 50 °C, 17% RH, and 1 m s^{-1} wind speed for 90 min (Vallerand et al., 1992). Volunteers were semi-nude and at rest. Skin temperatures were measured with an infrared radiometer at 10 locations. The mean skin temperature was reported along with rectal and auditory canal temperatures. Mean skin temperature was estimated with a weighted average of 10 measured skin temperatures. The measured and predicted values are shown in Fig. 7. The predicted rectal and ear temperatures are

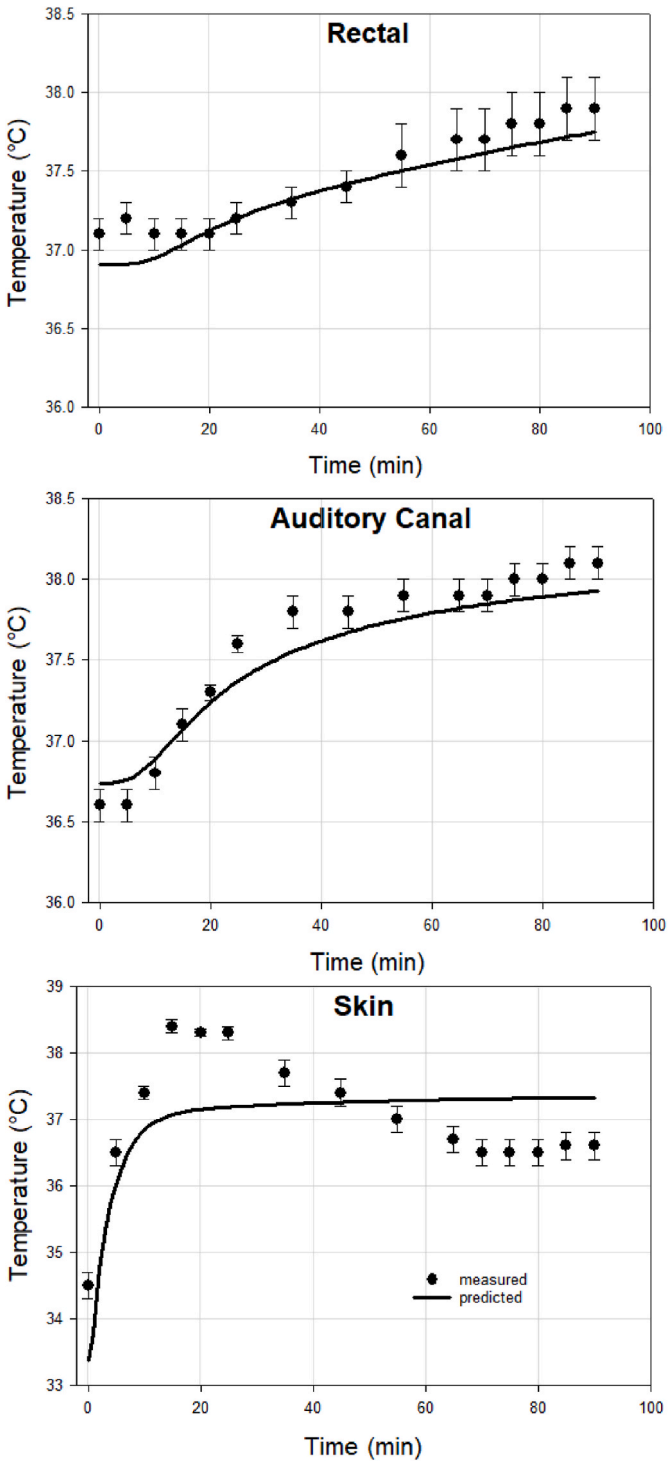

Fig. 7. Predicted and measured rectal, auditory canal, and skin temperatures in an environment of 50 °C, 17% RH, and 1 m s^{-1} wind speed (*Vallerand et al. 1992*).

near one SD of the mean measured temperature for a majority of the measurement points. The RMSD of the core was 0.14 °C. The predicted skin temperature did not fully follow the same pattern as those observed, but the RMSD was 0.81 °C. The trend of the measured skin temperature appears different from those observed in studies at similar conditions where skin temperatures increased and then reached a steady-state value (Webb 1992; Stolwijk 1971).

3.4. Exercise in warm conditions

Twenty-four female volunteers exercised on a semi-recumbent cycle ergometer at metabolic rates of 135 and 200 W m^{-2} ($Q_{EX_{tot}}$ = 94 and 183 W respectively) in an environment of 28 °C, 36% RH, and a wind speed <0.5 m s^{-1} (Notley et al., 2017). The volunteers wore a torso singlet, shorts, socks, and shoes, and started with a 20 min rest, followed by 45 min of exercise, and 20 min recovery. Skin temperatures at eight sites and auditory canal temperatures were measured. Fig. 8 shows the predicted and measured auditory canal and mean skin temperature at the two metabolic rates. The model predicted the auditory canal temperature well, but consistently over predicted the mean skin temperature especially during recovery from exercise at a heat production of 200 W m^{-2}. Overall, the RMSD was 0.2 °C for the auditory temperature and 0.8 °C for the skin temperatures.

3.5. Exercise in hot environment

Four female volunteers walked on a treadmill at 0.89 m s^{-1} (2 mph) at a 2% grade in an environment of 36 °C, 64% RH and a 0.5 m s^{-1} wind speed for 90 min (Avellini et al., 1980). The rectal and skin temperatures at 6 sites were measured. Estimates of metabolic heat production from exercise ($Q_{EX_{tot}}$) were 205 W using the Pandolf equation (Pandolf et al., 1977). Fig. 9 shows the results of the predicted and measured rectal and skin temperatures. Predicted mean skin temperatures agree with the measured temperatures. The model under predicts the rectal temperature consistently by ~0.3 °C, although the tendency of the predicted rectal temperature follows the measured value well over time. The initial measured rectal temperature was ~37.25 °C while the initial value of the model was 36.91 °C. The model has a RMSD of 0.28 °C for the predicted rectal temperatures and 0.30 °C for the predicted skin temperatures.

3.6. Summary

Table 5 shows the RMSD for each comarison between the predicted and mesured values for each study and the average RMSD when all studies are equally weighted. The RMSD for the core temperature and the mean skin temperature are 0.2 °C and 0.69 °C, respectively.

4. Discussion

A finite element model of thermoregulation in female was successfully developed. To the best of our knowledge, this is the first thermoregulation model that uses a realistic female body as the passive system. The passive system was constructed with the geometrically and anatomically accurate XCAT Phantoms, containing 13 tissue types. The complexity and sophistication of the model geometry allows for temperature predictions across the entire body with higher spatial resolution than any available systems of which we are aware.

The model was validated using multiple published data sets during exercise and rest in thermoneutral, cold, and hot environments. Predicted core and mean and local skin temperatures were compared to the measured values. The predicted core temperatures were in close agreement (within 1 SD) with observed values in most cases. Most of the predicted local skin temperatures were also in good agreement with the measured values as was mean skin temperature. Inter-and intra-individual differences exist in the reported temperatures. For example, with the data used for the validation, initial core temperatures ranged from 36.6 °C to 37.3 °C and initial mean skin temperatures varied from 31.1 °C to 34.5 °C. When evaluating the performance of a thermoregulatory model in hot and cold environments, a 0.5 °C difference in core temperature and a 1.6 °C difference in mean skin temperature are considered in good agreement and acceptable (Haslam and Parsons 1994). Thus, this geometrically and anatomically correct finite element model predicts local temperatures in women within acceptable limits.

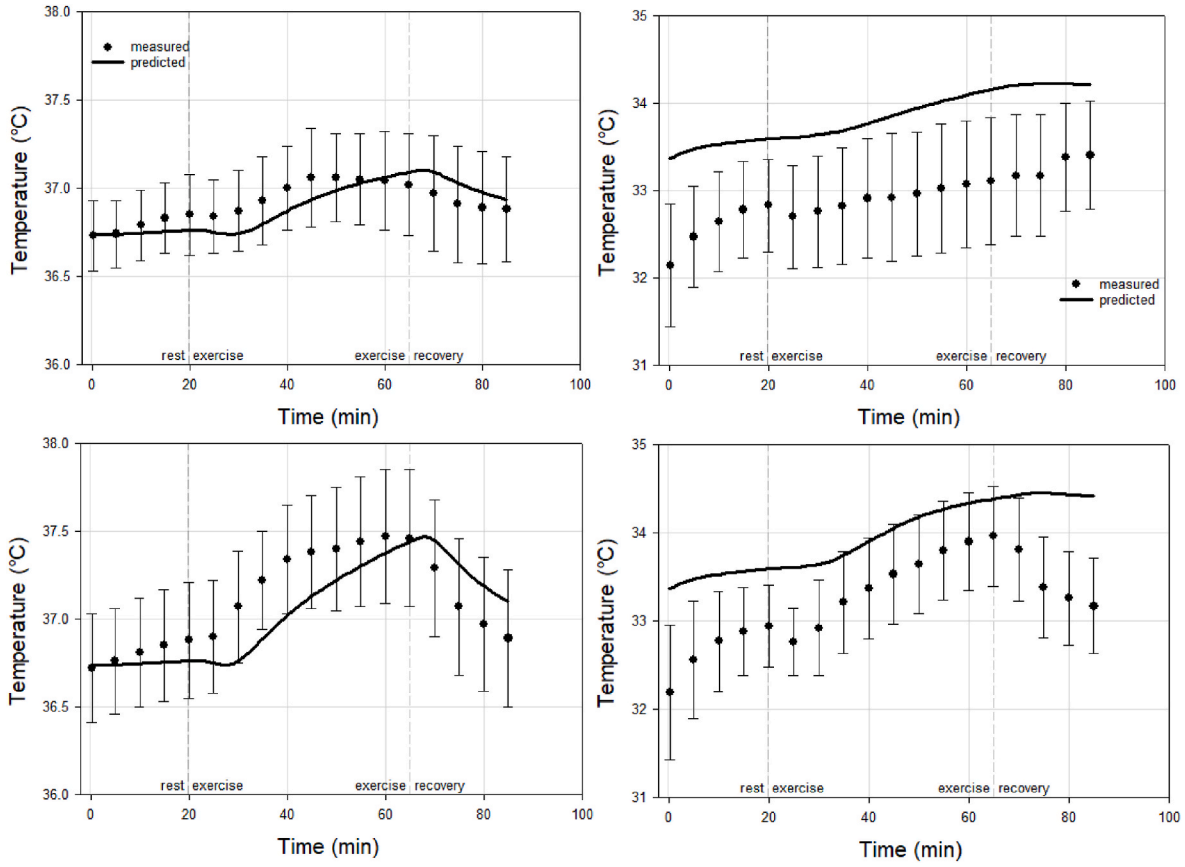

Fig. 8. Predicted and measured auditory (left) and mean skin (right) temperatures when exercising at 135 W m^{-2} (top) and 200 W m^{-2} (bottom) in an environment of 28 °C, 36% RH, and 0.1 m s^{-1} wind speed *(Notley et al. 2017)*.

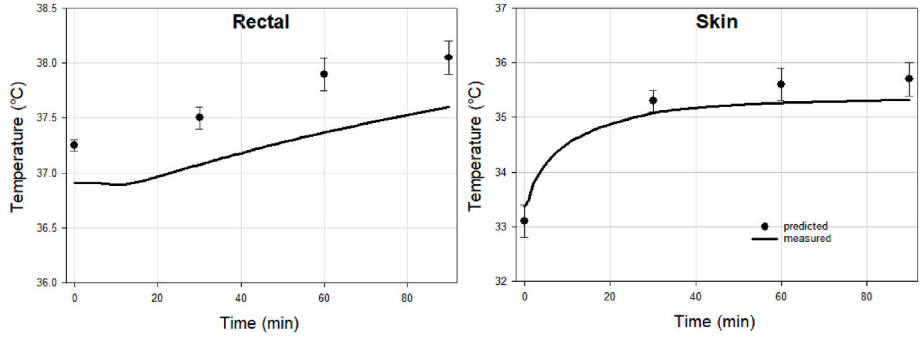

Fig. 9. Predicted and measured rectal (left) and mean skin temperatures (right) while wearing exercise clothing, exercising in 36 °C, 64% RH and a 0.5 m s^{-1} wind *(Avellini et al. 1980)*.

Table 5
RMSE for the predicted core and mean skin temperatures for each study.

Study	Core	Mean Skin
Olesen	0.09	0.57
Nonaka		0.42
Castellani	0.28	1.24
Vallerand	0.14	0.81
Notley	0.20	0.80
Avellini	0.28	0.30
Average	0.20	0.69

Passive systems to model human thermoregulation have been consistently advancing, primarily by increasing the complexity of the human body geometry. Representation of the human body has evolved initially from a one-cylinder approximation to six-cylinder and greater compartments and most recently to more complicated geometries (Xu and Tikuisis 2014; Havenith and Fiala 2015; Kang et al., 2019; Ludwig et al., 2008; Silva et al., 2016). The progressively increasing complexity allows the researcher to represent the human body more definitively, and thus more accurately predict temperature with greater spatial resolution. For example, the popular two-node model for thermal comfort predicted 2 temperatures (Gagge et al., 1972), the Stolwijk and Hardy model predicted 24 body temperatures (Stolwijk 1971), and some models predict local temperatures at ~180 locations (Fiala et al., 1999). The resolution has been improving, but is still relatively low for certain applications. For example, most of the multi compartment models do not predict finger temperatures. However, finger temperature is important in thermoregulation, highly associated with mean body temperature and

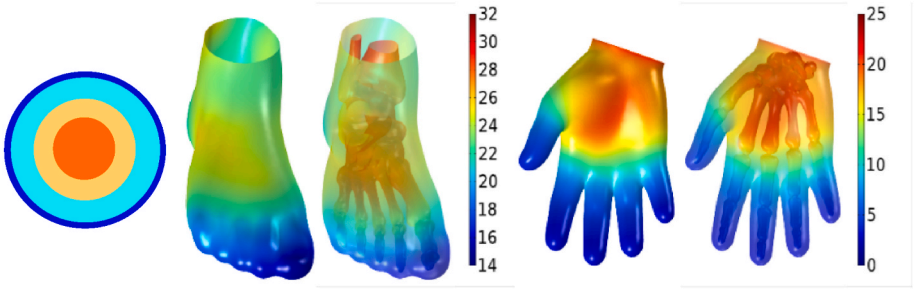

Fig. 10. The temperature distribution predicted by cylinder-based models (left). Foot and hand temperatures in a 0 °C environment are shown during simulation using the finite element thermoregulatory model (middle and right).

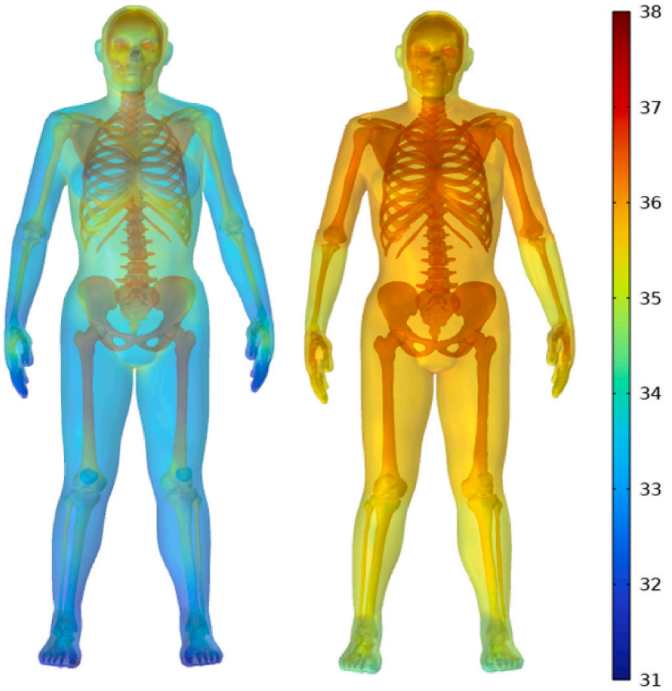

Fig. 11. Predicted skin and bone temperatures in thermoneutral (left) and hot (right) environments.

manual dexterity performance, and potentially a good indicator of thermal comfort and heat balance (Koscheyev et al., 2005; Kim 2009; Zhang et al., 2021; Cartwright et al., 2022).

The passive system of the current model is realistic and quantitatively based on actual human female anatomy allowing our new model to predict spatial temperatures at significantly higher resolutions. Fig. 10 (left) schematically shows core, muscle fat and skin temperatures predicted four-layer cylinder based models, and the prediction shows radial variation only. Fig. 10 (middle and right) shows the temperature distributions across the right foot and hand during sedentary exposure in 0 °C air using the FETM. The foot has skin temperatures ranging from 14.7 to 26.1 °C with a bone temperature range of 16.2–30.3 °C. The hand skin temperature ranges from 2.5 to 20.8 °C and a bone temperature range of 3–24.5 °C. Fig. 11 shows the spatial distribution of the skin and bone temperatures across the body. The results in Figs. 10 and 11 demonstrate this female model is capable of not only predicting core and skin temperatures as existing compartment models do, but also predicts spatial organ and tissue temperatures at high resolution.

Many researchers have studied differences in thermoregulation between males and females during exposures to heat and cold, but conclusions are limited, and more research is needed (Yanovich et al., 2020; Gagnon and Kenny 2012). Models of thermoregulation in women are potentially useful tools to study the sex differences in thermoregulation and analyze potential mechanisms for such differences. The results in Fig. 3 reveals that predicted female temperatures differed slightly from the predicted male values in thermoneutral conditions. The skin temperatures predicted by the current female model were further compared to the skin temperatures predicted by the male model in two dynamic conditions (wearing cold ensemble and resting at 0 °C and while resting in a 40 °C environment, Fig. 12). The male and female mean skin temperatures are similar in 40 °C environment. However, the female skin temperature is lower than the male temperature in 0 °C environment and their differences increased gradually over time. Summaries of studies on sex differences in the responses to cold stress shows that female resting in cold environments had lower skin temperature (Stephenson and Kolka 1993; Graham 1988). Thus, this initial comparison demonstrates that the temperatures predicted by this female model are different than the temperatures predicted by the male models and the differences are consistent with observations.

In this model the finger is part of the hand and has the same thermoregulatory mechanisms as the hand (e.g., blood flow). This could be

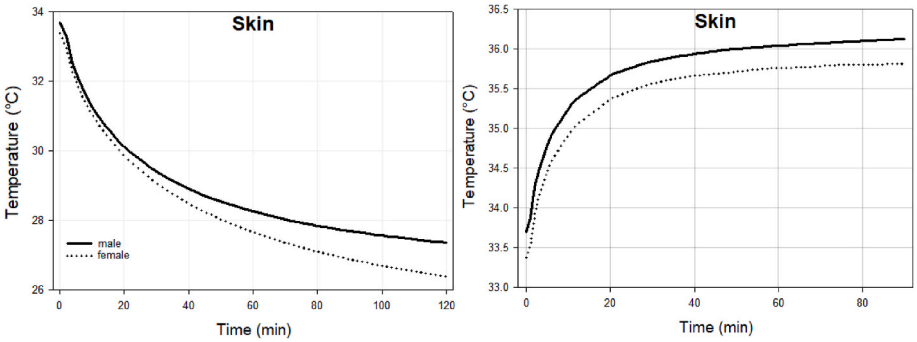

Fig. 12. Predicted male and female mean skin temperatures while wearing cold weather clothing ensemble and resting in 0 °C, RH 51%, 1.34 m s^{-1} (*Castellani et al. 2018*) and resting nude in an environment of 40 °C, 20% RH, and 0.18 m s^{-1} wind speed.

one reason that predicted finger temperature does not drop as quickly as the observed values in Fig. 6. It is necessary to separate the fingers from the hand so their differences in thermoregulatory mechanisms, e.g., cold-induced vasodilatation (CIVD), can be simulated more accurately.

This model has the potential to be used as a powerful tool for numerous applications where temperature gradients over the body are high for situations during exposure to widely disparate environments. For example, this model can be used to study therapeutic hypothermia after cardiac arrest and develop optimal treatment strategies (Xu and Tikuisis 2014; Skok et al., 2020). Another example is to use this model to evaluate female thermal responses and comfort in automobiles and office buildings (Fiala et al., 2010; Koelblen et al., 2018; Enescu 2019), to study potential uses of finger temperature as indices for control of HVAC systems, and to evaluate and optimize personal protective equipment, e.g., localized heating/cooling system, for female users. Finally, preventative guidance for hot and cold-weather conditions to reduce susceptibility to environmental injuries can specifically be developed for females, which has been lacking.

5. Limitations

A limitation of our present model is that the passive system was constructed using a female avatar of 36 years old, 1.62 m tall and 66 kg mass. However, the model was validated with mean values from a group rather than values from specific individuals. Therefore, the current model likely simulates the mean thermal responses of an "average" young female, but people with larger or smaller body sizes would require additional analyses to be more comprehensively and accurately modeled. Additionally, this model does not account for menstrual cycle effects and/or contraceptive use on thermoregulatory effector responses.

6. Conclusion

We present a novel female finite element model of human thermoregulation, which is anatomically and geometrically accurate for young healthy women with normal BMI and predicts spatial temperatures at a high resolution. The body mesh preserved 13 organs and tissues and maintained their geometrical shapes. Thus, this model provides a much higher degree of spatial resolution and anatomical realism compared to existing compartment- or layer-based models. The model was validated against human data from rest and exercising conditions under thermoneutral, hot, and cold conditions. Validation showed that the model predicted core and local skin temperatures with acceptable accuracy. The average RMSD of 0.2 °C for core temperatures and 0.69 °C for skin temperatures.

Funding

There is no funding to report.

CRediT authorship contribution statement

Michael P. Castellani: Conceptualization, development, Validation, Writing – original draft, preparation. **Timothy P. Rioux:** Conceptualization, development, reviewing and editing. **John W. Castellani:** physiology data acquisition, contribution to development/validation, reviewing and editing. **Adam W. Potter:** contribution to development, reviewing and editing. **Sean R. Notley:** physiology data acquisition, contribution to validation, reviewing and editing. **Xiaojiang Xu:** Supervision, Conceptualization, development, Validation, Writing – original draft, preparation, All authors approved the final manuscript.

Declaration of competing interest

The author declares that there are no conflicts of interest.

Acknowledgments

The authors would like to thank Dr. Nisha Charkoudian for her critical review of this paper. The authors would like to thank Drs. Chris Goddard, Ross Cotton, and Kerim Genc (Synopsys, CA) for developing the female body mesh and expert support, and Dr. Nagi Elabbasi and Dr. Andrew Spann (Veryst Engineering, MA) for their assistance with the COMSOL software.

Approved for public release; distribution is unlimited. The opinions or assertions contained herein are the private views of the author(s) and are not to be construed as official or reflecting the views of the Army or the Department of Defense. Any citations of commercial organizations and trade names in this report do not constitute an official Department of the Army endorsement of approval of the products or services of these organizations.

Annex. Regional thermal and evaporative resistances

Tables 6 and 7 show regional thermal and evaporative resistances required for simulation. The values for Castellani data were measured (Xu et al., 2021), and rest were estimated based on the description in the papers and the similar values in our clothing database.

Table 6
Regional thermal resistances (clo) values for each study

Region	Olesen	Nonaka	Castellani	Vallerand	Notley	Avellini
Head	0	0	1	0	0	0
Torso	0.82	0.82	2.65	0	0.6	0
Upper arm	0.71	0.71	2.27	0	0	0
Forearm	0.46	0.46	2.27	0	0	0
Hand	0	0	0.2	0	0	0
Thigh	0.59	0.59	0.69	0	0.6	0
Lower leg	0.43	0.43	0.69	0	0	0
Foot	0.46	0.46	1.02	0	1.2	0

Table 7
Regional evaporative resistances ($m^2 \cdot Pa \cdot W^{-1}$) values for each study

Region	Olesen	Nonaka	Castellani	Vallerand	Notley	Avellini
Head	0	0	5.1	0	0	0
Torso	19.2	19.2	103.8	0	10.0	0
Upper arm	26.2	26.3	76.2	0	0	0
Forearm	13.9	13.9	76.2	0	0	0
Hand	0	0	2.3	0	0	0
Thigh	29.9	29.9	36.1	0	10.0	0
Lower leg	15.8	15.8	36.1	0	0	0
Foot	48.8	48.8	79.9	0	36.0	0

References

Ackerman, M.J., 1999. The visible human Project: a resource for education. Acad. Med. 74 (6), 667–670.

ASHRAE, 2013. Thermal comfort. In: 2013 ASHRAE Handbood Fundamentals. American Society of Heating, Refrigerating and Air Conditioning Engineers, Atlanta, 9.1-9.9.32.

Avellini, B., Kamon, E., Krajewski, J., 1980. Physiological responses of physically fit men and women to acclimation to humid heat. J. Appl. Physiol. 49 (2), 254–261.

Cartwright, J.M.T., Etter, C.V., Gnatiuk, E.A., Perrotta, A.S., Wang, F., White, M.D., 2022. Duration limits for exposure for the whole body and extremities with a military extreme cold protection clothing ensemble at an ambient temperature of -40°C. Temperature 9 (2), 211–222. https://doi.org/10.1080/23328940.2022.2078635.

Castellani, J.W., Yurkevicius, B.R., Jones, M.L., Driscoll, T.J., Cowell, C.M., Smith, L., Xu, X., O'Brien, C., 2018. Effect of localized microclimate heating on peripheral skin temperatures and manual dexterity during cold exposure. J. Appl. Physiol. 125 (5), 1498–1510.

Castellani, M.P., Rioux, T.P., Castellani, J., Potter, A.W., Xu, X., 2021. A geometrically accurate 3 dimensional model of human thermoregulation for transient cold and hot environments. Comput. Biol. Med. https://doi.org/10.1016/j.compbiomed.2004.01.004. S0010482504000290 [pii], ([doi]).

Charkoudian, N., Hart, E.C., Barnes, J.N., Joyner, M.J., 2017. Autonomic control of body temperature and blood pressure: influences of female sex hormones. Clin. Auton. Res. 27 (3), 149–155.

Choudhary, B., Udayraj, Wang, F., Ke, Y., Yang, J., 2020. Development and experimental validation of a 3D numerical model based on CFD of the human torso wearing air ventilation clothing. Int. J. Heat Mass Tran. 147, 118973 https://doi.org/10.1016/j.ijheatmasstransfer.2019.118973.

Christ, A., Kainz, W., Hahn, E.G., Honegger, K., Zefferer, M., Neufeld, E., Rascher, W., Janka, R., Bautz, W., Chen, J., Kiefer, B., Schmitt, P., Hollenbach, H.P., Shen, J., Oberle, M., Szczerba, D., Kam, A., Guag, J.W., Kuster, N., 2010. The Virtual Family–development of surface-based anatomical models of two adults and two children for dosimetric simulations. Phys. Med. Biol. 55 (2), N23–N38.

de Dear, R.J., Arens, E., Hui, Z., Oguro, M., 1997. Convective and radiative heat transfer coefficients for individual human body segments. Int. J. Biometeorol. 40 (3), 141–156.

Enescu, D., 2019. Models and indicators to assess thermal sensation under steady-state and transient conditions. Energies 12 (5). https://doi.org/10.3390/en12050841.

Fanger, P.O., 1982. Thermal Comfort: Analysis and Applications in Environmental Engineering. RE Krieger Pub. Co.

Ferreira, M.S., Yanagihara, J.I., 2009. A transient three-dimensional heat transfer model of the human body. Int. Commun. Heat Mass Tran. 36 (7), 718–724. https://doi.org/10.1016/j.icheatmasstransfer.2009.03.010.

Fiala, D., Lomas, K.J., Stohrer, M., 1999. A computer model of human thermoregulation for a wide range of environmental conditions: the passive system. J. Appl. Physiol. 87 (5), 1957–1972.

Fiala, D., Lomas, K.J., Stohrer, M., 2001. Computer prediction of human thermoregulatory and temperature responses to a wide range of environmental conditions. Int. J. Biometeorol. 45 (3), 143–159.

Fiala, D., Psikuta, A., Jendritzky, G., Paulke, S., Nelson, D.A., Lichtenbelt, W.D., Frijns, A. J., 2010. Physiological modeling for technical, clinical and research applications. Front. Biosci. 2, 939–968. https://doi.org/10.2741/s112.

Gagge, A., Stolwijk, J., Nishi, Y., 1972. An effective temperature scale based on a simple model of human physiological regulatiry response. Memoir. Facul. Eng. 13 (Suppl. l), 21–36. Hokkaido University.

Gagge, A.P., Gonzalez, R.R., 2010. Mechanisms of heat exchange: biophysics and physiology. In: Compr Physiol 2011, Supplement 14: Handbook of Physiology, Environmental Physiology. John Wiley & Sons, Inc, pp. 45–84. https://doi.org/10.1002/cphy.cp040104. First published in print 1996. doi: 10.1002/cphy.cp.040104.

Gagnon, D., Kenny, G.P., 2011. Sex modulates whole-body sudomotor thermosensitivity during exercise. J. Physiol. 589 (Pt 24), 6205–6217. https://doi.org/10.1113/jphysiol.2011.219220.

Gagnon, D., Kenny, G.P., 2012. Does sex have an independent effect on thermoeffector responses during exercise in the heat? J. Physiol. 590 (23), 5963–5973. https://doi.org/10.1113/jphysiol.2012.240739.

Genc, K.O., Segars, P., Cockram, S., Thompson, D., Horner, M., Cotton, R., Young, P., 2013. Workflow for creating a simulation ready virtual population for finite element modeling. J. Med. Dev. Trans. ASME 7 (4).

Graham, T.E., 1988. Thermal, metabolic, and cardiovascular changes in men and women during cold stress. Med. Sci. Sports Exerc. 20 (5), S185–S192.

Haslam, R.A., Parsons, K.C., 1994. Using computer-based models for predicting human thermal responses to hot and cold environments. Ergonomics 37 (3), 399–416. https://doi.org/10.1080/00140139408963659 ([doi]).

Havenith, G., Fiala, D., 2015. Thermal indices and thermophysiological modeling for heat stress. Compr. Physiol. 6 (1), 255–302.

Huizenga, C., Hui, Z., Arens, E., 2001. A model of human physiology and comfort for assessing complex thermal environments. Build. Environ. 36 (6), 691–699. https://doi.org/10.1016/S0360-1323(00)00061-5.

Iyoho, A.E., Ng, L.J., MacFadden, L., 2017. Modeling of gender differences in thermoregulation. Mil. Med. 182 (Suppl. l_1), 295–303. https://doi.org/10.7205/MILMED-D-16-00213.

Kang, Z., Wang, F., Udayraj, 2019. An advanced three-dimensional thermoregulation model of the human body: development and validation. Int. Commun. Heat Mass Tran. 107, 34–43.

Karaki, W., Ghaddar, N., Ghali, K., Kuklane, K., Holmer, I., Vanggaard, L., 2013. Human thermal response with improved AVA modeling of the digits. Int. J. Therm. Sci. 67, 41–52, 0.

Kim, J.H., 2009. Optimization of Cooling Regimes in a Liquid Cooling Garment (LCG) to Support Thermal Balance and Comfort of the Human Body during Exercise. PhD Thesis. University of Minnesota Minneapolis, MN.

Kingma, B.R.M., Steenhoff, H., Toftum, J., Daanen, H.A.M., Folkerts, M.A., Gerrett, N., Gao, C., Kuklane, K., Petersson, J., Halder, A., Zuurbier, M., Garland, S.W., Nybo, L., 2021. ClimApp—integrating personal factors with weather forecasts for individualised warning and guidance on thermal stress. Int. J. Environ. Res. Publ. Health 18 (21). https://doi.org/10.3390/ijerph182111317.

Koelblen, B., Psikuta, A., Bogdan, A., Annaheim, S., Rossi, R.M., 2018. Human simulator – a tool for predicting thermal sensation in the built environment. Build. Environ. 143, 632–644. https://doi.org/10.1016/j.buildenv.2018.03.050.

Koscheyev, V.S., Leon, G.R., Coca, A., 2005. Finger heat flux/temperature as an indicator of thermal imbalance with application for extravehicular activity. Acta Astronaut. 57 (9), 713–721. https://doi.org/10.1016/j.actaastro.2005.03.063.

Lai, D., Chen, Q., 2016. A two-dimensional model for calculating heat transfer in the human body in a transient and non-uniform thermal environment. Energy Build. 118, 114–122.

Lamke, L.O., Nilsson, G.E., Reithner, H.L., 1977. Insensible perspiration from the skin under standardized environmental conditions. Scand. J. Clin. Lab. Investig. 37 (4), 325–331. https://doi.org/10.3109/00365517709092637.

Lamke, L.O., Wedin, B., 1971. Water evaporation from normal skin under different environmental conditions. Acta Derm. Venereol. 51 (2), 111–119.

Ludwig, M., Koch, J., Fischer, B., 2008. An application of the finite volume method to the bio-heat-transfer-equation in premature infants. Electron. Trans. Numer. Anal. 28, 136–148.

Mehnert, P., Bröde, P., Griefahn, B., 2002. Gender-related difference in sweat loss and its impact on exposure limits to heat stress. Int. J. Ind. Ergon. 29, 343–351. https://doi.org/10.1016/S0169-8141(02)00073-2.

Nelson, D.A., Charbonnel, S., Curran, A.R., Marttila, E.A., Fiala, D., Mason, P.A., Ziriax, J. M., 2009. A high-resolution voxel model for predicting local tissue temperatures in humans subjected to warm and hot environments. J. Biomech. Eng. 131 (4), 041003 https://doi.org/10.1115/1.3002765.

Nonaka, M., Ueno-Towatari, T., Ohnaka, T., 2009. Differences between mean and local skin temperatures with neutral thermal sensation and thermal comfort : a comparison of skin temperature differences among female students between in summer and in winter. J. Human Living Environ. 16 (2), 91–97. https://doi.org/10.24538/jhesj.16.2_91.

Notley, S.R., Park, J., Tagami, K., Ohnishi, N., Taylor, N.A., 2017. Variations in body morphology explain sex differences in thermoeffector function during compensable heat stress. Exp. Physiol. 102 (5), 545–562.

Olesen, B.W., Fanger, P.O., 1973. The skin temperature distribution for resting man in comfort. Arch. Sci. Physiol. 27 (4), 385–393.

Pandolf, K.B., Givoni, B., Goldman, R., 1977. Predicting energy expenditure with loads while standing or walking very slowly. J. Appl. Physiol. 43 (4), 577–581.

Pereira, C.B., Heimann, K., Czaplik, M., Blazek, V., Venema, B., Leonhardt, S., 2016. Thermoregulation in premature infants: a mathematical model. J. Therm. Biol. 62, 159–169. https://doi.org/10.1016/j.jtherbio.2016.06.021.

Potter, A.W., Looney, D.P., Santee, W.R., Gonzalez, J.A., Welles, A.P., Srinivasan, S., Castellani, M.P., Rioux, T.P., Hansen, E.O., Xu, X., 2020. Validation of new method for predicting human skin temperatures during cold exposure: the Cold Weather Ensemble Decision Aid (CoWEDA). Inform. Med. Unlocked 18, 100301.

Segars, W.P., Bond, J., Frush, J., Hon, S., Eckersley, C., Williams, C.H., Feng, J., Tward, D.J., Ratnanather, J.T., Miller, M.I., Frush, D., Samei, E., 2013. Population of anatomically variable 4D XCAT adult phantoms for imaging research and optimization. Med. Phys. 40 (4), 043701.

Silva, A.B.C.G., Laszczyk, J., Wrobel, L.C., Ribeiro, F.L.B., Nowak, A.J., 2016. A thermoregulation model for hypothermic treatment of neonates. Med. Eng. Phys. 38 (9), 988–998. https://doi.org/10.1016/j.medengphy.2016.06.018.

Silva, A.B.C.G., Wrobel, L.C., Ribeiro, F.L.B., 2018. A thermoregulation model for whole body cooling hypothermia. J. Therm. Biol. 78, 122–130. https://doi.org/10.1016/j.jtherbio.2018.08.019.

Skok, K., Duh, M., Stožer, A., Markota, A., Gosak, M., 2020. Thermoregulation: A Journey from Physiology to Computational Models and the Intensive Care Unit. Wiley Interdiscip Rev Syst Biol Med. https://doi.org/10.1002/wsbm.1513 e1513.

Stephenson, L.A., Kolka, M.A., 1993. Thermoregulation in women. Exerc. Sport Sci. Rev. 21, 231–262.

Stolwijk, J.A.J., 1971. A Mathematical Model of Physiological Temperature Regulation in Man (Washington, D.C).

Stolwijk, J.A.J., Hardy, J.D., 2011. Control of body temperature. In: Compr Physiol 2011, Supplement 26: Handbook of Physiology, Reactions to Environmental Agents. John Wiley & Sons, Inc, pp. 45–68. https://doi.org/10.1002/cphy.cp090104. First published in print 1977. DOI: 10.1002/cphy.cp.090104.

Sun, X., Eckels, S., Zheng, Z.C., 2012. An Improved Thermal Model of the Human Body. Paper Presented at the HVAC&R Research, 6/1/2012.

Takahashi, Y., Nomoto, A., Yoda, S., Hisayama, R., Ogata, M., Ozeki, Y., Tanabe, S-i, 2021. Thermoregulation model JOS-3 with new open source code. Energy Build. 231, 110575 https://doi.org/10.1016/j.enbuild.2020.110575.

Tan, A.P., Cheong, C.H., Lee, T., Seng, K.Y., Teo, C.J., 2021. Computer modelling of heat strain responses of exercising personnel in tropical climate. Comput. Biol. Med. 134, 104530 https://doi.org/10.1016/j.compbiomed.2021.104530.

Tanabe, S-i, Kobayashi, K., Nakano, J., Ozeki, Y., Konishi, M., 2002. Evaluation of thermal comfort using combined multi-node thermoregulation (65MN) and radiation models and computational fluid dynamics (CFD). Energy Build. 34 (6), 637–646. https://doi.org/10.1016/S0378-7788(02)00014-2.

Tikuisis, P., Giesbrecht, G.G., 1999. Prediction of shivering heat production from core and mean skin temperatures. Eur. J. Appl. Physiol. Occup. Physiol. 79 (3), 221–229.

Tikuisis, P., Jacobs, I., Moroz, D., Vallerand, A.L., Martineau, L., 2000. Comparison of thermoregulatory responses between men and women immersed in cold water. J. Appl. Physiol. 89 (4), 1403–1411.

Unnikrishnan, G., Hatwar, R., Hornby, S., Laxminarayan, S., Gulati, T., Belval, L.N., Giersch, G.E.W., Kazman, J.B., Casa, D.J., Reifman, J., 2021. A 3-D virtual human thermoregulatory model to predict whole-body and organ-specific heat-stress responses. Eur. J. Appl. Physiol. https://doi.org/10.1007/s00421-021-04698-1.

Vallerand, A.L., Savourey, G., Hanniquet, A.-M., Bittel, J.H., 1992. How should body heat storage be determined in humans: by thermometry or calorimetry? Eur. J. Appl. Physiol. Occup. Physiol. 65 (3), 286–294.

Wan, X., Fan, J., 2008. A transient thermal model of the human body-clothing-environment system. J. Therm. Biol. 33 (2), 87–97. https://doi.org/10.1016/j.jtherbio.2007.11.002.

Webb, P., 1992. Temperatures of skin, subcutaneous tissue, muscle and core in resting men in cold, comfortable and hot conditions. Eur. J. Appl. Physiol. Occup. Physiol. 64 (5), 471–476. https://doi.org/10.1007/BF00625070.

Werner, J., Buse, M., 1988. Temperature profiles with respect to inhomogeneity and geometry of the human body. J. Appl. Physiol. 65 (3), 1110–1118.

Xu, X., Amin, M., Santee, W.R., 2008. Probability of Survival Decision Aid (PSDA). US Army Research Institute of Environmental Medicine, Natick, MA.

Xu, X., Berglund, L.G., Cheuvront, S.N., Endrusick, T.L., Kolka, M.A., 2004. Model of human thermoregulation for intermittent regional cooling. Aviat Space Environ. Med. 75 (12), 1065–1069.

Xu, X., Gonzalez, J.A., Santee, W.R., Blanchard, L.A., Hoyt, R.W., 2016. Heat strain imposed by personal protective ensembles: quantitative analysis using a thermoregulation model. Int. J. Biometeorol. 60 (7), 1065.

Xu, X., Rioux, T.P., Gonzalez, J., Hansen, E.O., Castellani, J.W., Santee, W.R., Karis, A.J., Potter, A.W., 2021. A digital tool for prevention and management of cold weather injuries-Cold Weather Ensemble Decision Aid (CoWEDA). Int. J. Biometeorol. 65 (8), 1415–1426. https://doi.org/10.1007/s00484-021-02113-0.

Xu, X., Rioux, T.P., Pomerantz, N., Tew, S., 2019. Effects of fabric on thermal and evaporative resistances of chemical protective ensembles: measurement and quantification. Measurement 136, 248–255.

Xu, X., Tikuisis, P., 2014. Thermoregulatory modeling for cold stress. Compr. Physiol. 4 (3), 1057–1081.

Xu, X., Tikuisis, P., Gonzalez, R., Giesbrecht, G., 2005. Thermoregulatory model for prediction of long-term cold exposure. Comput. Biol. Med. 35 (4), 287–298. https://doi.org/10.1016/j.compbiomed.2004.01.004. S0010482504000290 [pii];, ([doi]).

Xu, X., Turner, C.A., Santee, W.R., 2011. Survival time prediction in marine environments. J. Therm. Biol. 36 (6), 340–345. https://doi.org/10.1016/j.jtherbio.2011.06.009.

Xu, X., Werner, J., 1997. A dynamic model of the human/clothing/environment-system. Appl. Human. Sci. 16 (2), 61–75.

Yanovich, R., Ketko, I., Charkoudian, N., 2020. Sex differences in human thermoregulation: relevance for 2020 and beyond. Physiology 35 (3), 177–184. https://doi.org/10.1152/physiol.00035.2019.

Zhang, H., Huizenga, C., Arens, E., Yu, T., 2001. Considering individual physiological differences in a human thermal model. J. Therm. Biol. 26, 401–408.

Zhang, M., Li, R., Li, J., Wang, F., Subramaniam, S., Lang, J., Passalacqua, A., Song, G., 2021. A 3D multi-segment thermoregulation model of the hand with realistic anatomy: development, validation, and parametric analysis. Build. Environ. 201, 107964 https://doi.org/10.1016/j.buildenv.2021.107964.